

PAPER • OPEN ACCESS

## Twisted single-ring hollow-core fiber for broadband chiral detection in nanoliter volumes

To cite this article: Christof Helfrich *et al* 2026 *J. Phys. Photonics* **8** 015035

View the [article online](#) for updates and enhancements.

### You may also like

- [Near-field-driven radiative thermal dynamics in aperiodic photonic nanostructures](#)  
M Prado, A Manjavacas, F A Pinheiro et al.
- [Femtosecond laser processing of quartz wafers for precision cutting of tuning forks](#)  
Raffaele De Palo, Jaka Mur, Matevž Marš et al.
- [Observation of distinct bound states in the continuum in the strained type-II Dirac photonic lattices](#)  
Haixiang Wu, Weizhao Cheng, Ruichang Chen et al.



## PAPER

## OPEN ACCESS

RECEIVED  
23 October 2025REVISED  
18 December 2025ACCEPTED FOR PUBLICATION  
6 January 2026PUBLISHED  
22 January 2026

Original content from this work may be used under the terms of the [Creative Commons Attribution 4.0 licence](https://creativecommons.org/licenses/by/4.0/).

Any further distribution of this work must maintain attribution to the author(s) and the title of the work, journal citation and DOI.



# Twisted single-ring hollow-core fiber for broadband chiral detection in nanoliter volumes

Christof Helfrich<sup>1,2</sup> , Sonia Maniappan<sup>2</sup> , Michael H Frosz<sup>2</sup>, Raju Adhikary<sup>3</sup>, Sandro Colagioia<sup>4</sup>, Nicolas Y Joly<sup>1,2</sup>, Andrea Marini<sup>3</sup> and Francesco Tani<sup>2,5,\*</sup>

<sup>1</sup> Friedrich-Alexander-University Erlangen-Nürnberg, Staudtstr. 7, 91058 Erlangen, Germany

<sup>2</sup> Max Planck Institute for the Science of Light, Staudtstr. 2, 91058 Erlangen, Germany

<sup>3</sup> Department of Physical and Chemical Sciences, University of L'Aquila, Via Vetoio, 67100 L'Aquila, Italy

<sup>4</sup> Dompé farmaceutici S.p.A., via Campo di Pile, L'Aquila, Italy

<sup>5</sup> CNRS, UMR 8523-PhLAM-Physique des Lasers Atomes et Molécules, University of Lille, Lille F-59000, France

\* Author to whom any correspondence should be addressed.

E-mail: [francesco.tani@univ-lille.fr](mailto:francesco.tani@univ-lille.fr)

**Keywords:** hollow-core fiber, chiral, polarization, sensing

Supplementary material for this article is available [online](#)

## Abstract

The ongoing evolution of hollow-core fibers (HCFs) continues to inspire the development of optofluidic platforms with enhanced sensitivity and minimal sample requirements. Here, we utilize the intrinsic advantages of anti-resonant reflection HCFs—such as low optical loss and broadband transmission—to realize a twisted single-ring HCF (SR-HCF) tailored for polarization-sensitive chiral detection. We optimize the fiber geometry to ensure single-mode operation by strongly attenuating higher-order modes ( $>50$  dB  $m^{-1}$ ) while maintaining low loss for the fundamental mode ( $<0.1$  dB  $m^{-1}$ ) and reducing the sample volume to only  $\sim 660$  nl per 34 cm fiber length. By applying a constant twist along the fiber length, we minimize birefringence and ensure stable transmission of linear polarization states with polarization extinction ratios surpassing 38 dB. After injecting an aqueous solution of an optically active molecule, we measure its optical rotation at different wavelengths with millidegree-level sensitivity and remarkable robustness against misalignment. Measurements with different enantiomeric excess concentrations are in good agreement with independent liquid chromatography characterization.

## 1. Introduction

The ever-ongoing quest to enhance the sensitivity of compact and distributed optical sensors and lab-on-chip platforms has significantly benefited from the development of photonic crystal fibers and microstructured waveguides [1–5]. Compared to other platforms, fibers provide lower optical loss, which enables long interaction lengths of the light with the sample. They can be designed to enhance and control the relevant properties of light and offer a high level of integration with other technologies and techniques. Systems based on microstructured fibers can provide enhanced sensitivity while requiring reduced sample volumes at the nl-level. Because of this, they have found multiple applications in optofluidics and have been successfully used for sensing [2, 3, 6–8], monitoring [9] and enhancing chemical reactions [3], Raman spectroscopy [10–13], measuring electric and magnetic fields [14–16] and detecting the enantiomeric concentration of chiral substances [17].

Among the different types of microstructured waveguides, anti-resonant reflection hollow-core fibers (ARR-HCFs) are notable for providing broadband transmission spanning 100 s of THz with core diameters ranging from  $\sim 6$   $\mu m$  up to  $\sim 120$   $\mu m$ , which can be filled with gaseous and liquid samples with refractive indices lower or even higher than that of the surrounding glass structure [3, 18, 19]. In recent years, ARR-HCFs have been improved beyond imagination, with their loss achieving unprecedentedly small values even lower than standard telecom fiber [20, 21]. Furthermore, despite being intrinsically multimode, the structure of these weakly guiding fibers can be tailored to enhance the loss of higher

order modes (HOMs) and introduce linear and circular birefringence so as to provide effective single mode and polarization maintaining guidance over tens of meters lengths [22–25]. Nonetheless, the loss achieved so far for HOMs is still insufficient to ensure their suppression over sub-meter lengths typical in many optofluidic and sensing applications.

To take advantage of the long interaction length and small filling volume provided by HCFs, these must preserve all the relevant attributes of the guided light. Usually, over lengths on the order of tens of cm (typical of liquid sensing applications), the optical loss of  $< 1 \text{ dB m}^{-1}$  is negligible, so is Rayleigh scattering, and polarization crosstalk is caused mainly by HOMs. Their polarization varies across their profile, and as their excitation is highly sensitive to alignment, even modest beam-pointing instability causes substantial variations in their power content. Thus, ensuring total suppression of HOMs over the used fiber length is crucial for precise polarization measurements, such as sensing electric and magnetic fields and chiral discrimination. Additionally, the accuracy of these measurements, particularly over broad spectral regions, is easily impaired by birefringence, which depends on the waveguide geometry in a complex manner and exhibits a wavelength dependence in the phase retardance and rotation of the principal axis.

Here, we report the design and fabrication of a single-ring HCF (SR-HCF) for broadband and polarization-sensitive applications. We then demonstrate its use in the characterization of chiral solutions achieving refractive index discrimination  $\Delta n \sim 10^{-10}$  using a filling volume of only  $\sim 660 \text{ nl}$  per 34 cm fiber length. Compared to previous works employing HCFs [17], it represents an improvement by  $\sim 1000$  times in sensitivity, thus approaching that of commercial narrowband polarimeters and state-of-the-art broadband interferometric techniques [26], which employ sample volumes of several tens of microliters (or even larger).

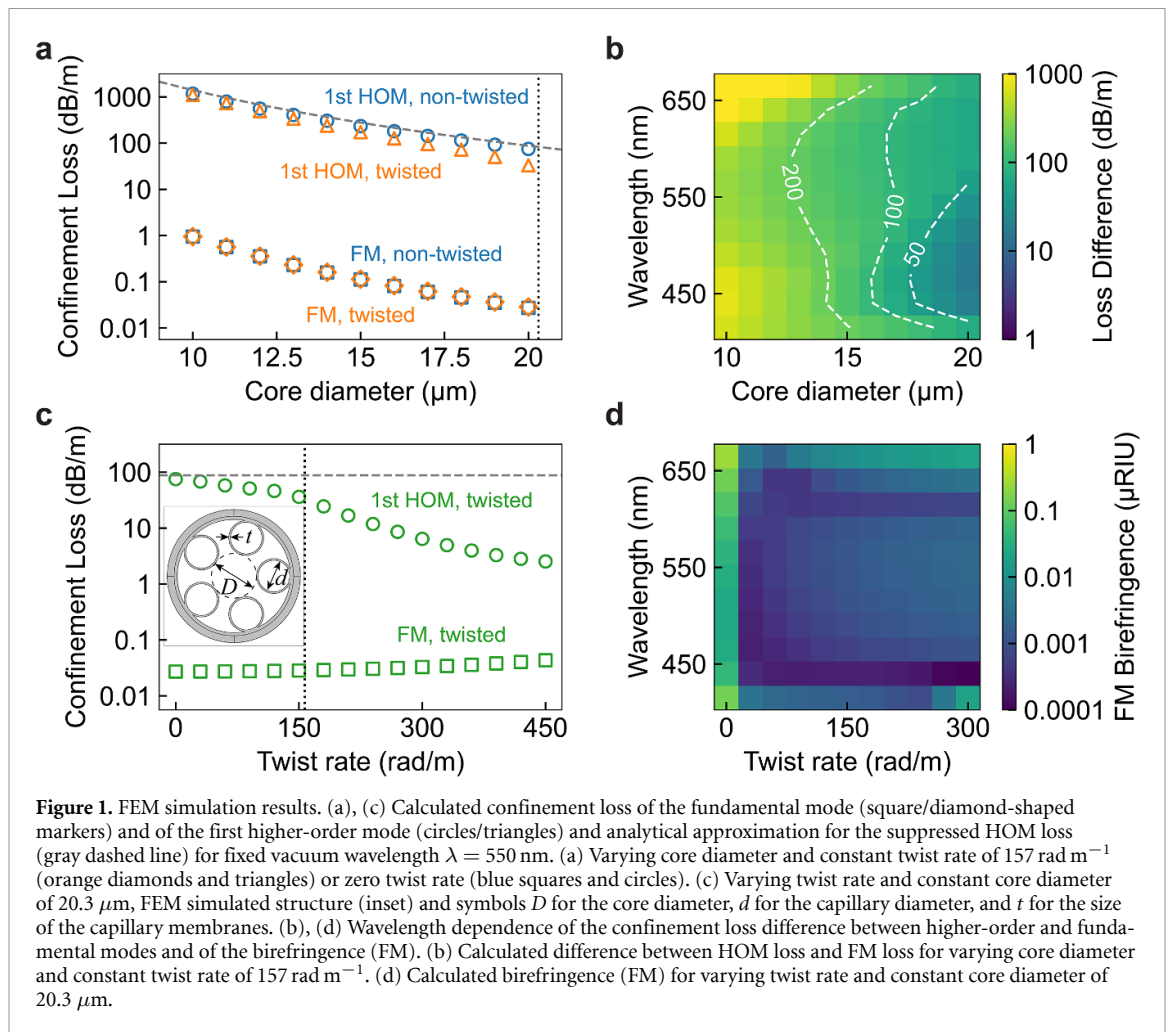
For this, we designed the waveguide to exhibit single-mode guidance (with unprecedentedly high loss for the HOMs), low birefringence, and preserve the polarization of the guided light to an exceptional degree over tens of cm. First, we describe the waveguide design and its optical properties, and then the characterization of the fabricated fiber in the second part. Finally, in the last section, we report measurements of the optical rotation (OR) of the guided light induced by an aqueous solution containing a chiral drug and benchmark the experimental results with independent liquid chromatography measurements and numerical simulations.

## 2. Fiber design

In light of the above discussion, a waveguide for applications in optofluidics and chiral sensing should ensure: (1) effectively single-mode guidance, (2) preservation of the polarization state of the light, (3) low birefringence, and (4) broadband guidance coinciding with the transmission window of common solvents. The latter can be attained by opportunely selecting the spectral position of the anticrossing between the core-guided light and the capillary-wall modes determined by

$$\lambda_m = (2t/m) \sqrt{n_g^2 - n_c^2}, \quad (1)$$

where  $t$  is the thickness of the capillaries surrounding the core,  $n_g$  and  $n_c$  are the refractive indices of the glass and of the core-filling medium and  $m$  is an integer number [27]. Common solvents (water, ethanol, hexane, acetonitrile) transmit well in the visible region and have similar refractive indices, and guidance in this spectral range can be obtained by selecting  $t \sim 235 \text{ nm}$  or  $t \sim 700 \text{ nm}$ , which are achievable thicknesses for the capillary walls of SR-HCFs. Single-mode guidance and preservation of the polarization state have been reported previously, but only over long lengths (several meters) [20, 22–24] and the latter either by introducing birefringence or over a narrow spectral region ( $< 5 \text{ THz}$ ) [23, 28]. Effectively single-mode SR fibers can be realized by choosing [22]  $d/D \sim 0.68 \dots 0.70$  (the exact value depends on the number of capillaries), where  $D$  and  $d$  are the diameters of the core and the surrounding capillaries, and by twisting the fiber along its axis [24]. Fibers with this aspect ratio provide a leak channel for the core-guided HOMs (via phase-matching these to the fundamental modes of the surrounding capillaries) greatly enhancing their confinement losses. These have approached  $\sim 20 \text{ dB m}^{-1}$  in reported waveguides [20, 22, 24], a value, however, too low to avoid HOM contamination over sub-meter lengths. A recipe to achieve much higher loss is revealed by the suppressed HOM loss coefficient  $\alpha_{\text{sHOM}} = (20 \cdot \lambda^3)/d^4 \text{ [dB m}^{-1}\text{]}$  (confinement loss, where  $\lambda$  is the light vacuum wavelength), which is approximately valid for a fused silica SR-HCF filled with water or air (in the SI we give the derivation of this result). Thus, for visible light, HOM loss approaching or even exceeding  $100 \text{ dB m}^{-1}$  can be obtained by reducing the core diameter below  $20 \mu\text{m}$ . This is shown in figures 1(a) and (b), where we plot the confinement loss of the modes supported by a 5-capillary fiber, calculated via finite element



modeling (FEM, modeled fiber structure shown in the inset of figure 1(c),  $t = 670$  nm,  $d/D = 0.7$ ). We notice that in the case of SR-HCFs, 5-capillary geometries provide the optimal compromise for enhancing the HOM loss without significantly affecting the fundamental mode loss. When  $D$  and  $t$  are fixed, fibers with  $< 5$  capillaries exhibit higher loss for the fundamental mode (FM), while  $> 5$  capillaries fibers support a larger number of HOMs with low loss over sub-meter lengths (see SI for details). In figure 1(a), we show the confinement loss of the fundamental mode and the first HOM (with azimuthal mode index  $|\ell| = 1$  and the lowest HOM loss, see SI) calculated via FEM simulation at 550 nm for a varying core diameter (open symbols) along with the HOM loss calculated using the above-given expression, and in figure 1(b) we illustrate the loss coefficient difference of these two modes as a function of the core diameter and the light wavelength. The plots reveal that for the selected geometry and  $D < 20 \mu\text{m}$ , we can realize SR-HCFs supporting a FM with loss below  $1 \text{ dB m}^{-1}$  and HOMs with loss above  $100 \text{ dB m}^{-1}$  over broad spectral ranges.

Ideal SR-HCFs exhibit zero birefringence [29], but in real fibers, it is typically non-zero ( $10^{-8} < \Delta n_{\text{eff}} < 10^{-6}$ ) due to geometry variations, which are unavoidable during fabrication [23]. Although the fiber birefringence is still small, it is not negligible, especially for optical activity measurement for which often the refractive index difference is  $< 10^{-9}$ . This is because the birefringence, its spectral dependence, and the rotation of the principal polarization axis contribute to the degradation of the polarization state of the guided light, thus reducing the sensitivity to tiny variations in polarization. We avoid this detrimental effect by spinning the preform during the fiber drawing to imprint a permanent twist that is uniform across the entire fiber length. By gaining an ‘average circular symmetry’ of the fiber [30, 31], twisting provides a viable route to reduce the fiber birefringence to values  $< 10^{-9}$ . Our analysis confirms, that this is highly robust against perturbations to the waveguide geometry (see supplementary information). In figure 1(d), we show the difference in the effective index of the two fundamental modes (i.e. the birefringence) supported by the fiber shown in the inset of figure 1(c) and calculated via FEM accounting for realistic variations of the structure, which were estimated using scanning electron microscope (SEM) images of fabricated fibers (RMS error  $\sim 96$  nm for the five capillary diameters in

the fiber cross section and RMS error  $\sim 14$  nm for the thicknesses, see SI for more details). The simulation results in figure 1(d) show that the waveguide birefringence and its wavelength dependence reduce significantly even for a moderate twist rate. In the transition region (not shown here), the birefringence decreases at twist rates in the order of  $1 \text{ rad m}^{-1}$  until a minimum is reached (at  $\sim 10 \text{ rad m}^{-1}$ ), which is followed by a linear increase that has been reported in previous works [32]. Whereas the confinement loss of the fundamental mode is almost unaffected by variations in the twist rate, the confinement loss for some HOMs decreases significantly when the twist rate exceeds a given threshold. This can be seen in figure 1(c), where we show the calculated confinement loss for the FM and the first HOM (with azimuthal mode index  $|\ell| = 1$  and the lowest HOM loss) with the latter decreasing rapidly for a twist rate above  $150 \text{ rad m}^{-1}$ . Above this threshold, HOM suppression is increasingly affected by twist-induced non-degenerate mode splitting [33], and the fiber exhibits helical dichroism as recently reported [34] and does not ensure any more single-mode guidance over short lengths (see SI for further details).

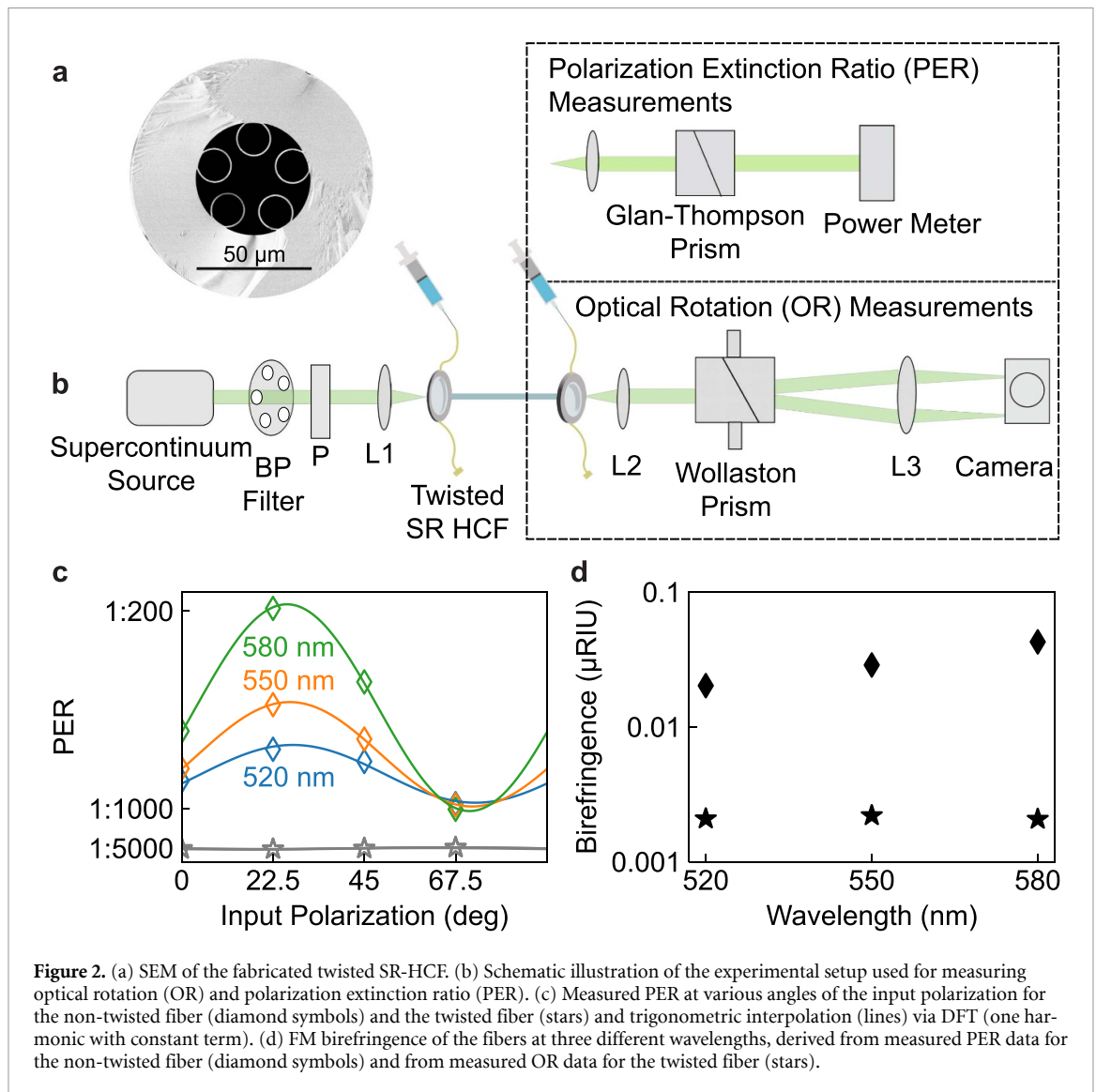
### 3. Fiber characterization and optical setup

In figure 2(a), we show the SEM image of the fiber that we fabricated following the design discussed in the previous section, along with (b) a sketch of the optical setup, which we used for its characterization and for the optical activity measurements. We use light at 520 nm, 550 nm, and 580 nm obtained by filtering the output of a supercontinuum source (see SI for details) with 10-nm bandpass filters. After one of these, the light goes through a linear polarizer to ensure linear polarization. Subsequently, the light is launched into the SR-HCF whose end facets are placed in liquid cells with fused silica windows so that it can be filled with the desired solution. For the in-coupling of the light, we use an achromatic lens of focal length 25 mm achieving a 70% transmission (corresponding to 75% transmission when accounting for Fresnel reflection at the liquid cell windows), and a  $10\times$  microscope objective (focal length 16 mm) to collimate the output. The light then passes through a Glan Thompson prism, which is rotated to determine the minimum and maximum power. The minimum and maximum output power were measured using a power meter and their ratio was used to calculate the polarization extinction ratio (PER). Using this optical setup, we characterized the PER at the output of  $\sim 30$  cm-long pieces of the SR-HCF ( $d/D \approx 0.7$ ,  $D \approx 20.3 \text{ }\mu\text{m}$ ,  $t \approx 670 \text{ nm}$ ) and a twisted version of it (twist rate of  $157 \text{ rad m}^{-1}$ ), both filled with water.

In figure 2(c), we show the PER measured at the output of these two fibers at the three wavelengths and as a function of the input polarization. The non-twisted fiber already preserves the polarization of light to a good degree, which indicates single-mode guidance (i.e. high loss for the HOMs). However, the waveguide also exhibits a pronounced dependence of PER on both wavelength and input polarization caused by birefringence. On the other hand, at the output of the twisted fiber, we measure  $\approx 38$  dB PER, which corresponds to an improvement by at least ten times with the setup's sensitivity being the main limit to the determination of the actual PER and its dependence on the wavelength and polarization of the input light. Furthermore, the measured PER is also affected by the light guided by the surrounding glass jacket, which is multimode and in a random polarization state [34]. To account for this and precisely measure the OR at the fiber output, we use the setup sketched in figure 2(b). After collimating the waveguide output, the light passes through a Wollaston prism placed in a rotational mount, after which the two orthogonal components are focused onto a Basler acA1920-40um CMOS sensor camera using a lens with a focal length of 400 mm. In this fashion, by recording images for different rotation angles of the Wollaston prism and excluding the pixels that lie outside the core mode, we can measure the OR of light with a maximum deviation from the mean value  $< 5$  millidegrees in a series of ten repeated measurements. Comparing measurements of the OR with and without the water-filled twisted fiber reveals that, although the waveguide rotates the light polarization by about 236 mdeg, such a background can be subtracted. Note that with low sample concentrations, background removal is more involved if the waveguide exhibits large linear birefringence.

Flushing and filling of the fiber and day-to-day variations introduce deviations of approximately 10 mdeg, which could either be attributed to mechanical stress due to pressure variation/relaxation, or to the manual sample injection and flushing process.

Further, we investigate the error introduced when impairing the optical alignment at the fiber input. Experimentally, we intentionally misalign the input light beam as much as to reduce the transmission by 50%. In a multimode fiber, this would cause strong transmission of HOMs, and consequently affect the polarization state in an irreproducible way. In our setup, the measured OR changed by only few tens of mdeg in response to the intentional misalignment, which confirms the good HOM suppression that we can already achieve with a large core diameter of  $20 \text{ }\mu\text{m}$ .



These data reveal an improvement in the sensitivity by  $\sim 1000$ -fold compared to the work of Schorn *et al* [17], which reported the use of ARR HCF for chiral discrimination for the first time. Furthermore, from our characterization of the system, we identify additional possible improvements, which include optimization of the sample injection process, increasing the thickness of the outer glass jacket to make the waveguide more resilient against mechanical stress and decreasing the core diameter. From the background OR of the twisted fiber, we derive the magnitude of its circular birefringence (in units of  $\mu\text{RIU}$ ), and in figure 2(d) we compare this result with the linear birefringence of the non-twisted fiber (derived from PER measurements). The measured waveguide birefringence is in good agreement with numerical simulations (see SI for details).

#### 4. Optical activity measurements and simulations

We use the fiber and the optical setup described in the previous section to measure (at room temperature) the OR induced by a water-based solution containing Ladarixin (DF2156A: 4-((1R)-1-methyl-2-((methylsulfonyl)amino)-2-oxoethyl)phenyl trifluoromethanesulfonate sodium salt) – a small chiral molecule inhibitor of the interleukin-8 receptor CXCR1 and CXCR2 [35–37]. We use a total concentration  $\sigma = \sigma_R + \sigma_S = 5 \text{ mg/ml}$  and different enantiomeric excess concentrations  $\sigma_R - \sigma_S$ , where  $\sigma_R$  ( $\sigma_S$ ) are the R (S) enantiomer concentration. The solutions were prepared and characterized by Dompé farmaceutici S.P.A. and the enantiomeric composition of each mixture was accurately determined by using high-performance liquid chromatography (HPLC) equipped with specifically selected chiral stationary phases, allowing for resolution and quantification of the individual enantiomers.

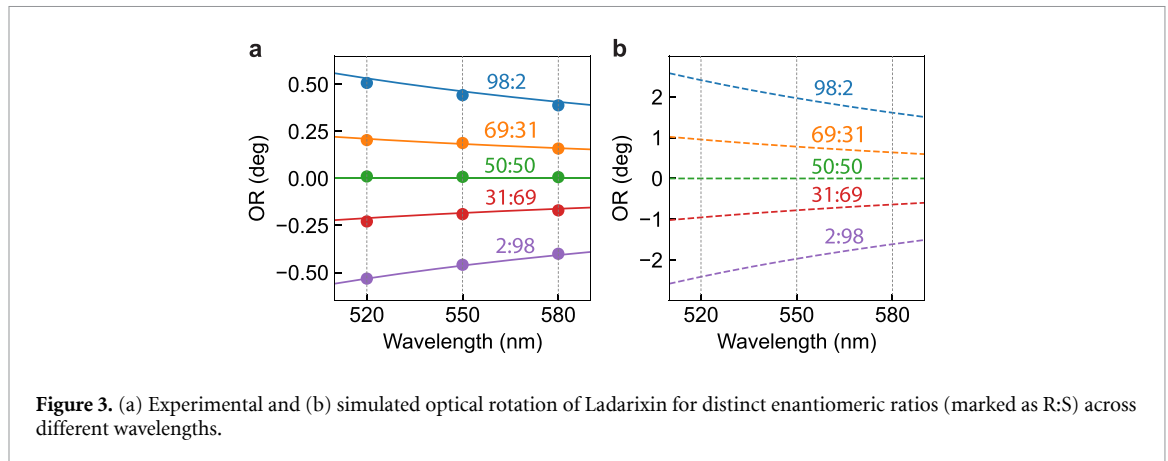


**Figure 3.** (a) Experimental and (b) simulated optical rotation of Ladarixin for distinct enantiomeric ratios (marked as R:S) across different wavelengths.

In figure 3(a), we show the OR measured at the output of a fiber piece of length  $L = 34$  cm (corresponding to  $\sim 660$  nl) and filled with solutions at varying enantiomeric ratios  $ee_R = (\sigma_R - \sigma_S)/(\sigma_R + \sigma_S)$  of the R and S enantiomers, which were independently characterized via liquid chromatography. The plot shows the data acquired using light at the three different wavelengths and after subtracting the OR caused by the weak circular birefringence of the twisted fiber. For the background removal, we use the same fiber piece filled with pure water and obtain the following OR values:  $-0.218$  deg at 580 nm,  $-0.244$  deg at 550 nm, and  $-0.245$  deg at 520 nm. We obtain OR values varying linearly with the enantiomeric excess, consistently increasing at shorter wavelengths, and as large as 0.54 deg at 520 nm. The plot displays mirror image data points for the same enantiomeric excess but with opposite signs, reflecting the expected relationship between OR and handedness. The OR data follow the curve

$$\theta_\lambda [\text{deg}] = \frac{A(T)}{\lambda^2 - \lambda_{\text{res}}^2} L \sigma ee_R, \quad (2)$$

where  $\lambda_{\text{res}} = 236$  nm is the molecular resonance wavelength obtained from numerical simulations (see below) and for the temperature  $T$  dependent term we use  $A(T) = 7.0 \text{ deg dm}^{-1} \text{ cm}^3 \text{ g}^{-1} \mu\text{m}^2$  obtained by fitting the data. We observe only minor deviations (smaller than 30 millidegrees) from the expected behavior (equation (2)), which are well within the errors of the liquid chromatography characterization. Furthermore, to verify that the chiral molecules are homogeneously distributed within the core and not attached to the extended inner core-walls surface or trapped in regions where the light does not travel, we measured the OR also using a 10 cm long cuvette and obtained consistent results.

We also compare the data with those obtained from theoretical simulations previously reported [38]. Quantum molecular observables (QMOs) (electric and magnetic dipole moments, electronic/vibrational transition energies, and relaxation rates) of the chiral drug solution are determined by employing a hybrid analytical/computational method. Semi-classical molecular dynamics simulations (to capture the Ladarixin-water conformational dynamics and highly probable conformational basins, obtained as minima of the Gibbs free energy), time-dependent density functional theory, and the perturbed matrix method are adopted to determine ensemble averages of the QMOs of Ladarixin in water. Furthermore, radiation-matter interaction is accounted for analytically by perturbatively solving density matrix equations of Ladarixin electrons within the electric/magnetic dipole approximation. Such calculations enable the evaluation of radiation-induced electric/magnetic dipole moments in every Ladarixin molecule, averaged over the high-probability molecular conformations [39]. In order to evaluate the macroscopic response of the chiral drug solution, we calculate the averaged induced electric/magnetic dipole moments over random molecular orientations through the Euler rotation matrix approach and the macroscopic polarization and magnetization vectors, related to electric and magnetic fields through electric/magnetic permittivity/permeability and the chiral parameter  $\kappa(\lambda)$  [38]. Thus, OR is calculated as

$$\theta_{\text{OR}}(\lambda) [\text{deg}] = \frac{2\pi L}{\lambda} \text{Re}[\kappa(\lambda)] \frac{180}{\pi}. \quad (3)$$

Results illustrated in figure 3(b) show that the sign of the experimental OR is in agreement with theoretical predictions (the R enantiomer is levorotatory, corresponding to a positive value  $\theta$ ).

We attribute the discrepancies between the experimental and simulated OR values shown in figure 3 to model assumptions. In the quantum chemistry simulations of the chiroptical response of solvated

Ladarixin, only the lowest-energy electronic and highest-energy vibrational transitions were included owing to computational constraints. Incorporating additional transitions would likely improve the quantitative agreement between theoretically predicted and experimentally obtained OR angles.

## 5. Conclusions

In conclusion, we have demonstrated a twisted SR-HCF optimized for polarization-sensitive measurements. Our work shows a clear route for the design of SR-HCFs with near-zero birefringence, which are polarization maintaining and single-mode over short lengths and over very broad spectral ranges. In particular, we have analyzed the optimal number of capillaries, adequate core diameters, and the permissible range of twist rates. The waveguide provides broadband guidance of light over extended lengths without altering the relevant properties for chiroptical studies (i.e. polarization state, spatial mode profile, and amplitude). As a result, the fiber can function as an ideal cuvette with a volume that increases linearly with its length and in the order of hundreds of nanoliters for an interaction length of tens of centimeters (for comparison, typical sub-microliter cuvettes provide path lengths of around  $100\ \mu\text{m}$ ). To realize the fiber, we engineered the waveguide geometry to increase the loss of HOMs to values of several tens of  $\text{dB m}^{-1}$  well beyond what was reported so far, thus effectively suppressing them after lengths of only a few tens of cm. Furthermore, by controlling the fiber twist rate, we could significantly reduce the waveguide birefringence over a broad spectral range, while arbitrary linear polarization states are transmitted mostly unchanged, except for a small residual circular birefringence of  $\Delta n_{\text{eff}} \approx 2.1 \times 10^{-9}$ . For comparison, the waveguide's linear birefringence without twisting is  $\Delta n_{\text{eff}} \approx 3.1 \times 10^{-8}$  (from PER measurements). Using this waveguide, we measured the OR of a water-based Ladarixin solution ( $5\ \text{mg ml}^{-1}$ ) over a broad spectral range (520–580 nm) for various enantiomeric ratios, achieving a sensitivity in the millidegree range via reliable background subtraction. With a filling volume as small as  $\sim 660\ \text{nl}$ , we measured OR exceeding 0.5 degrees in excellent agreement with those yielded by independent liquid chromatography measurements. Finally, we observed experimentally that the system is highly robust against optical misalignment, which is crucial for the future development of compact, sensitive, and versatile platforms for characterizing chiral solutions using minimal sample volumes, and potentially also for other applications such as low-noise supercontinuum generation [40–42], flying particle sensors [43, 44] and magnetic field sensing [15, 16].

## Data availability statement

The data that support the findings of this study are available upon reasonable request from the authors. Supporting information available at <https://doi.org/10.1088/2515-7647/ae340f/data1>.





## Acknowledgments

We acknowledge the European Innovation Council for funding through the Pathfinder Open TwistedNano (Grant No. 101046424). We thank Dompé Farmaceutici SpA for HPLC measurements of solvated Ladarixin.

## Conflict of interest

The authors filed a patent on the design of the fiber discussed in the article. S.C. is employed by Dompé farmaceutici s.p.a., which developed Ladarixin and holds the original patent for the molecule.

## ORCID iDs

Christof Helfrich  0009-0008-0550-2065  
Sonia Maniappan  0000-0003-4507-2641  
Andrea Marini  0000-0003-2763-6394  
Francesco Tani  0000-0001-6482-0647

## References

- [1] Shao L, Liu Z, Hu J, Gunawardena D and Tam H Y 2018 *Micromachines* **9** 145
- [2] Testa G, Persichetti G and Bernini R 2024 *TRAC Trends Anal. Chem.* **178** 117865
- [3] Cubillas A M, Unterkofler S, Euser T G, Etzold B J M, Jones A C, Sadler P J, Wasserscheid P and Russell P S J 2013 *Chem. Soc. Rev.* **42** 8629–48

- [4] Rindorf L, Jensen J B, Dufva M, Pedersen L H, Høiby P E and Bang O 2006 *Opt. Express* **14** 8224–31
- [5] Vaiano P, Carotenuto B, Pisco M, Ricciardi A, Quero G, Consales M and Crescitelli A Esposito E and Cusano A 2016 *Laser Photonics Rev.* **10** 922–61
- [6] Nissen M, Doherty B, Hamperl J, Kobelke J, Weber K, Henkel T and Schmidt M A 2018 *Sensors* **18** 478
- [7] Khozayemeh F, Melli F, Capodaglio S, Corradini R, Benabid F, Vincetti L and Cucinotta A 2022 *Sensors* **22** 5144
- [8] Wei J et al 2025 *ACS Photonics* **12** 5312–44
- [9] Cubillas A M, Schmidt M, Scharrer M, Euser T G, Etzold B J M, Taccardi N, Wasserscheid P and Russell P S J 2012 *Chem. Eur. J.* **18** 1586–90
- [10] Yang X, Zhang A Y, Wheeler D A, Bond T C, Gu C and Li Y 2012 *Anal. Bioanal. Chem.* **402** 687–91
- [11] Yan D, Popp J, Pletz M W and Frosch T 2017 *ACS Photonics* **4** 138–45
- [12] Eravuchira P J, Banchelli M, D'Andrea C, Angelis M D, Matteini P and Gannot I 2020 *J. Biomed. Opt.* **25** 077001
- [13] Groom M J et al 2024 *ACS Photonics* **11** 3167–77
- [14] Michie A, Canning J, Bassett I, Haywood J, Digweed K, Ashton B, Stevenson M, Digweed J, Lau A and Scandurra D 2007 *Meas. Sci. Technol.* **18** 3070
- [15] Thakur H V, Nalawade S M, Gupta S, Kittere R and Kale S N 2011 *Appl. Phys. Lett.* **99** 161101
- [16] Alberto N, Domingues M F, Marques C, André P and Antunes P 2018 *Sensors* **18** 4325
- [17] Schorn F, Essert A, Zhong Y, Abdullayev S, Castiglione K, Haumann M and Joly N Y 2023 *Anal. Chem.* **95** 3204–9
- [18] Fokoua E N, Mousavi S A, Jasion G T, Richardson D J and Poletti F 2023 *Adv. Opt. Photonics* **15** 1–85
- [19] Amrani F, Osório J H, Delahaye F, Giovanardi F, Vincetti L, Debord B, Jérôme F and Benabid F 2021 *Light: Sci. Appl.* **10** 7
- [20] Gao S, Chen H, Sun Y, Xiong Y, Yang Z, Zhao R, Ding W and Wang Y 2025 *Optica* **12** 56–61
- [21] Petrovich M et al 2025 *Nat. Photon.* **19** 1203–8
- [22] Uebel P, Günendi M C, Frosz M H, Ahmed G, Edavalath N N, Ménard J M and Russell P S J 2016 *Opt. Lett.* **41** 1961–4
- [23] Taranta A, Numkam Fokoua E, Abokhamis Mousavi S, Hayes J R, Bradley T D, Jasion G T and Poletti F 2020 *Nat. Photon.* **14** 504–10
- [24] Edavalath N N, Günendi M C, Beravat R, Wong G K L, Frosz M H, Ménard J M and Russell P S J 2017 *Opt. Lett.* **42** 2074–7
- [25] Roth P, Chen Y, Günendi M C, Beravat R, Edavalath N N, Frosz M H, Ahmed G, Wong G K L and Russell P S J 2018 *Optica* **5** 1315–21
- [26] Ghosh S, Herink G, Perri A, Preda F, Manzoni C, Polli D and Cerullo G 2021 *ACS Photonics* **8** 2234–42
- [27] Archambault J L, Black R, Lacroix S and Bures J 1993 *J. Lightwave Technol.* **11** 416–23
- [28] Fini J M, Nicholson J W, Mangan B, Meng L, Windeler R S, Monberg E M, DeSantolo A, DiMarcello F V and Mukasa K 2014 *Nat. Commun.* **5** 5085
- [29] Steel M J, White T P, Sterke C M d, McPhedran R C and Botten L C 2001 *Opt. Lett.* **26** 488–90
- [30] Barlow A J, Ramskov-Hansen J J and Payne D N 1981 *Appl. Opt.* **20** 2962–8
- [31] Galtarossa A, Palmieri L and Schenato L 2008 *J. Lightwave Technol.* **26** 3660–8
- [32] Weiss T, Wong G K L, Biancalana F, Barnett S M, Xi X M and Russell P S J 2013 *J. Opt. Soc. Am.* **30** 2921–7
- [33] Russell P S, Beravat R and Wong G K L 2017 *Phil. Trans. R. Soc. A* **375** 20150440
- [34] Helfrich C, Frosz M H and Tani F 2025 *ACS Photonics* **12** 564–9
- [35] Piro G et al 2023 *Br. J. Cancer* **128** 331–41
- [36] Piemonti L et al 2022 *Diabetes, Obesity Metab.* **24** 1840–9
- [37] Castelli V, Brandolini L, d'Angelo M, Giorgio C, Alfonso M, Cocchiario P, Lombardi F, Cimini A and Allegretti M 2021 *Cells* **10** 2324
- [38] Adhikary R et al 2025 *Sci. Rep.* **15** 13116
- [39] Venturi M et al 2023 *J. Chem. Phys.* **159** 154703
- [40] Lippl M, Frosz M H and Joly N Y 2023 *Opt. Lett.* **48** 5297–300
- [41] Sabbah M, Mears R, Harrington K, Wadsworth W J, Stone J M, Birks T A and Travers J C 2025 *J. Phys. Photon.* **7** 025019
- [42] Dudley J M, Genty G, Heidt A, Sylvestre T, Travers J C and Taylor J R 2025 *Europhys. Lett.* **151** 55001
- [43] Schmidt O A, Euser T G and Russell P S J 2013 *Opt. Express* **21** 29383–91
- [44] Freitag J, Schmidt P, Borandegi M, Redwig T and Schmauss B 2025 *29th Int. Conf. on Optical Fiber Sensors* vol 13639 (SPIE) pp 205–8 (available at: [www.spiedigitallibrary.org/conference-proceedings-of-spie/13639/136391L/Distributed-electric-field-measurements-along-a-hollow-core-fiber-by/10.1117/12.3061732.full](http://www.spiedigitallibrary.org/conference-proceedings-of-spie/13639/136391L/Distributed-electric-field-measurements-along-a-hollow-core-fiber-by/10.1117/12.3061732.full))